Rock Mechanics and Rock Engineering (2023) 56:6357–6374
https://doi.org/10.1007/s00603-023-03396-y

ORIGINAL PAPER

Analysis of the Historic Bondi Pumping Chamber Case Study Using the Adjusted Voussoir Beam Analog

Rami Abousleiman[1] · Sankhaneel Sinha[2,3] · Gabriel Walton[3]

Received: 10 January 2023 / Accepted: 17 May 2023 / Published online: 4 June 2023

Abstract

Analytical methods in engineering design use simplifying assumptions to reduce the number of variables considered for a given problem. In rock engineering design, this reduction in complexity increases practical applicability but often must be applied with a degree of conservatism, as relevant mechanisms may remain unaccounted for in a given analytical solution. To date, the voussoir beam analog has seen relatively limited application to complex roof stability problems. Previous research by the authors has used numerical modeling to expand the voussoir beam analog by developing analytical solution adjustments to account for important factors such as horizontal bedding and passive bolts. This paper presents the application of the adjusted voussoir beam analytical solution in a case study of the historic Bondi Pumping Chamber. Discrete element method numerical models are also presented to elucidate the mechanisms governing stability and deflection of the supported roof beam. The results of this study provide a novel real-world validation of the adjusted voussoir beam analog and insight into its practical applicability and limitations.

Highlights

- Successful field application of a voussoir beam analytical solution that accounts for supported flat-roof excavations in discontinuous rockmasses
- Effects of roof support installation timing and variations in discontinuity strength and stiffness identified through numerical models
- Self-supporting capacity of flat-roof excavations explored through comparison of numerical and analytical results

Keywords Voussoir beam analog · Discrete element method · Bolted roofs · Discontinuous rockmass · Case study · Bondi pumping chamber

List of Symbols

E	Young's modulus
s_j	Joint spacing
j_{kn}	Joint normal stiffness
E_{rm}	Rockmass modulus
E_{rmn}	Adjusted rockmass modulus
C	Scaling coefficient
n	Number of passively bolted layers
T_i	Individual layer thickness
T_e	Effective beam thickness

✉ Rami Abousleiman
rabousle@gmail.com

[1] Knight Piésold and Co., Denver, CO, USA

[2] WSP, Phoenix, AZ, USA

[3] Colorado School of Mines, Golden, CO, USA

1 Introduction

From its inception, the voussoir beam analog has been applied successfully in the design and study of roof stability in underground excavations. Widely credited to Evans (1941), who built on the work of Fayol (1885), it has since been studied via empirical (Wright and Mirza 1963; Talesnick et al. 2007; Tsesarsky 2012), analytical (Wright 1972; Beer and Meek 1982; Sofianos 1996; Diederichs and Kaiser 1999; Brady and Brown 2013; Yiouta-Mitra and Sofianos 2018), and numerical (Wright 1972; Ran et al. 1994;

Sofianos and Kapenis 1998; Alejano et al. 2008; Zhang et al. 2012; Oliveira and Pells 2014; Shabanimashcool and Li 2015; He and Zhang 2015; Oliveira and Paramaguru 2016; Carvalho and Carter 2020) methods. However, its application remains limited to specific rockmass conditions and excavation geometries. Specifically, the accurate application of the voussoir beam analog has historically been limited to simplified unsupported flat-roof excavations in discontinuous and layered rockmasses with low in-situ or excavation-induced horizontal stresses.

Analytical solutions for excavation roof displacement and stresses based on the voussoir beam analog allow the user to assess the self-supporting capacity of a jointed rock roof beam. Using relatively simple inputs related to roof span geometry and elastic material properties, users can calculate the maximum expected displacement and horizontal stress development using either closed-form (Sofianos 1996) or iterative loop (Diederichs and Kaiser 1999) calculations. The maximum displacement and horizontal stress can then be used to assess the roof beam's resistance to buckling, crushing, sliding, and tensile cracking failure (Sofianos 1996; Diederichs and Kaiser 1999).

Previous research has investigated the failure modes for different roof beam inclination angles (Zhang et al. 2012; He and Zhang 2015) and developed methods that can account for the effect of inclined roof beams, consider active support or surcharge pressure, or incorporate empirical rockmass rating systems to represent more complex rockmass conditions (Diederichs and Kaiser 1999). Others have presented methods of accounting for the presence of pre-tensioned bolted layers and in-situ horizontal stresses (Oliveira and Pells 2014; Oliveira and Paramaguru 2016). Shabanimashcool and Li (2015) also used numerical methods to evaluate the locked-in horizontal stresses in single-joint voussoir beams. Carvalho and Carter (2020) reworked the voussoir beam analytical solution found in Diederichs and Kaiser (1999) to analyze crown pillar stability (i.e. low span-to-thickness voussoir beams) and compared their analytical method to Finite Element Analysis model results. These existing methods of analyzing more complex voussoir beam behavior, while novel, have practical limitations. Notably, they do not directly account for the effect of multiple passively bolted layers, which can be found in both civil and mining excavation roofs. There have been some limited studies investigating the stabilization mechanism of rockbolts in laminated rockmasses (e.g. He and Zhang 2015), but an approach to account for this reinforcement effect in the voussoir analytical solution has not been historically available.

Most recently, the authors of this study developed an adjusted voussoir beam analytical method based on that of Diederichs and Kaiser (1999), which allows for multiple passively bolted roof layers to be considered. The Abousleiman et al. (2021) method was developed based on a statistical analysis of 810 unique discrete element method (DEM) numerical models and is summarized in Sect. 2.

The historic Bondi Pumping Chamber case study was identified as a suitable case study to evaluate the ability of the adjusted analytical method to estimate beam deflections consistent with those observed in reality. The Bondi Pumping Chamber excavation was advanced through competent, horizontally bedded, and cross-jointed sedimentary rock with a flat-roof geometry supported by 24 mm diameter, fully grouted roof bolts on 1.2 m square spacing. Additionally, the shallow nature of the excavation and its close proximity (i.e. ~ 30 m) to an unconfined escarpment make the loading conditions as close to the suite of bolted voussoir beam models analyzed by Abousleiman et al. (2021) as naturally possible. Specifically, the development of the unconfined cliff face through uplift and erosion has dissipated stored horizontal stress in the local rockmass (Pells 1993). The high strength of the rockmass relative to the in-situ stress magnitudes, coupled with the negligible horizontal stresses allows for independent evaluation of the in-situ impacts of discontinuities and support on the adjusted voussoir beam analog.

Previously, engineers who developed the excavation design utilized finite element method (FEM) numerical models and the voussoir beam analog (i.e. linear arch theory) with a significantly reduced Young's Modulus input and overestimated triangular surcharge load (i.e. 120 kPa peak) for a "conservative approach" (Pells 1993). With the development of the adjusted voussoir beam analog in Abousleiman et al. (2021), a more repeatable and rational approach can be applied to the Bondi Pumping Chamber to determine the appropriate degree of Young's modulus reduction.

Additionally, multiple two-dimensional (2D) discrete element method (DEM) numerical models of the Bondi Pumping Chamber excavation were developed to better understand the mechanics of the bolted voussoir beam and the effects of changes in rockmass conditions, installed support, and construction sequence. Model results also served as an additional comparison to the adjusted voussoir beam analog, allowing more thorough exploration of limitations and applications. Successful application of the adjusted voussoir beam analog to the Bondi Pumping Chamber case study is the first step towards more fully understanding how the adjusted analytical method can be applied to underground mines and civil excavations with more complex stress regimes, rockmass conditions, excavation geometries, and installed support.

2 The Adjusted Analytical Method

The adjusted analytical method of Abousleiman et al. (2021) is based on the voussoir beam analog solution of Diederichs and Kaiser (1999) and was developed using idealized bolted and bedded beam DEM numerical models that considered various bedding thicknesses (i.e. horizontal joint spacing), numbers of bolted layers, bolt spacings, vertical (i.e. cross) joint spacings, block material stiffnesses, joint stiffnesses, and bolt stiffnesses and strengths. This section briefly introduces the adjusted analytical method.

The Diederichs and Kaiser (1999) method alters the intact rock Young's Modulus (E) of a single roof beam based on the joint spacing (s_j) and joint stiffness (j_{kn}) to calculate a rockmass modulus (E_{rm}):

$$\frac{1}{E_{rm}} = \frac{1}{E} + \frac{1}{(jkn)s_j} \tag{1}$$

The adjusted method used further reduces the rockmass modulus to a new value (E_{rmn}) from the value calculated using Eq. (1) (E_{rm}) to account for the presence of passive roof support and the number of distinct layers (i.e. beds) using a scaling coefficient (C):

$$E_{rmn} = (C)E_{rm} \tag{2}$$

The relationship between number of passively bolted layers with fully penetrating bolts (n) and scaling coefficient is calculated according to the following relationship:

$$\mathrm{C} = \frac{1.1}{n^2} \tag{3}$$

E_{rmn} and the full thickness of the bolted interval are then input into the iterative loop solution from Diederichs and Kaiser (1999) to obtain the maximum displacement. However, stress arching of multi-layered bolted beams is often limited to individual layers, depending on the overall stiffness of the bolted beam and individual layer thickness (T_i). Therefore, to calculate the maximum horizontal stress in the beam, the iterative loop of Diederichs and Kaiser (1999) is rerun with an effective thickness (T_e) calculated as:

$$\frac{T_e}{T_i} = 0.19 \times \frac{1}{\sqrt{E_{rmn}}} + 1.05 \tag{4}$$

Stiffer beams (i.e. stiffer intact material, less jointed and layered beams, or more densely bolted) result in a lower effective thickness ratio.

The displacement and stress results from the adjusted analytical method can then be used to calculate buckling limit, factor of safety against crushing ($FoS_{crushing}$) and sliding ($FoS_{sliding}$) failure as described by Diederichs and Kaiser (1999).

3 Site Location & Geologic Setting

The Bondi Pumping Chamber is a 17 m deep, 70 m long, 19 m high, 12.5 m span flat-roof excavation completed in 1989 in Sydney, New South Wales, Australia (Pells and Best 1991). It is primarily utilized in support of water treatment and ocean sewer outfall operations at the Bondi Sewage Treatment Plant (STP) (McQueen 2004; Nye et al. 2005). The Bondi STP is one of three major ocean outfalls that pump treated sewage from the City of Sydney out into the Pacific Ocean (Fig. 1). The Bondi STP is located between Military Road and the edge of the coastal cliffs along the Pacific Ocean, north of the Bondi Golf and Diggers Club. The general site plan of the Bondi STP and the proposed location of the pumping chamber prior to its construction are also shown in Fig. 1. An isometric view of the Bondi STP from the northwest showing the location of the pumping chamber relative to other underground works is depicted in Fig. 2.

A generalized cross section of the outfall tunnel at Bondi STP and associated pumping chamber is shown in Fig. 3.

The pumping chamber was excavated in the Middle Triassic-age Hawkesbury Sandstone, which is a medium to coarse-grained quartz sandstone with minor shale and mudstone lenses (Pells 2004). The formation is subdivided into three facies with the "sheet" and "massive" sandstone facies comprising 95% of the formation, and the mudstone only 5% (Pells 2004). Cross-bedding in the sheet facies indicates that the Hawkesbury Sandstone was deposited in a fluvial delta system. An image of a typical Hawkesbury Sandstone outcrop from the North Head outfall tunnel project is shown in Fig. 4.

The material properties, roof displacement data, and construction sequence used for both the numerical model and the adjusted analytical solution were based on site-specific (Henderson and Windsor 1988; Pells and Best 1991; Nye et al. 2005) and regional (Bertuzzi and Pells 2002) information available in the literature, as well as personal communication with the engineer that assessed the original excavation using the voussoir beam analog (P. Pells, personal communication 03/23/21, 03/28/21, 04/03/21).

3.1 Construction and Instrumentation

The generalized excavation shape, support design, and surrounding geology of the Bondi Pumping Chamber excavation are shown in Fig. 5.

Figure 5, coupled with descriptions in Pells and Best (1991) allowed for a construction sequence, excavation

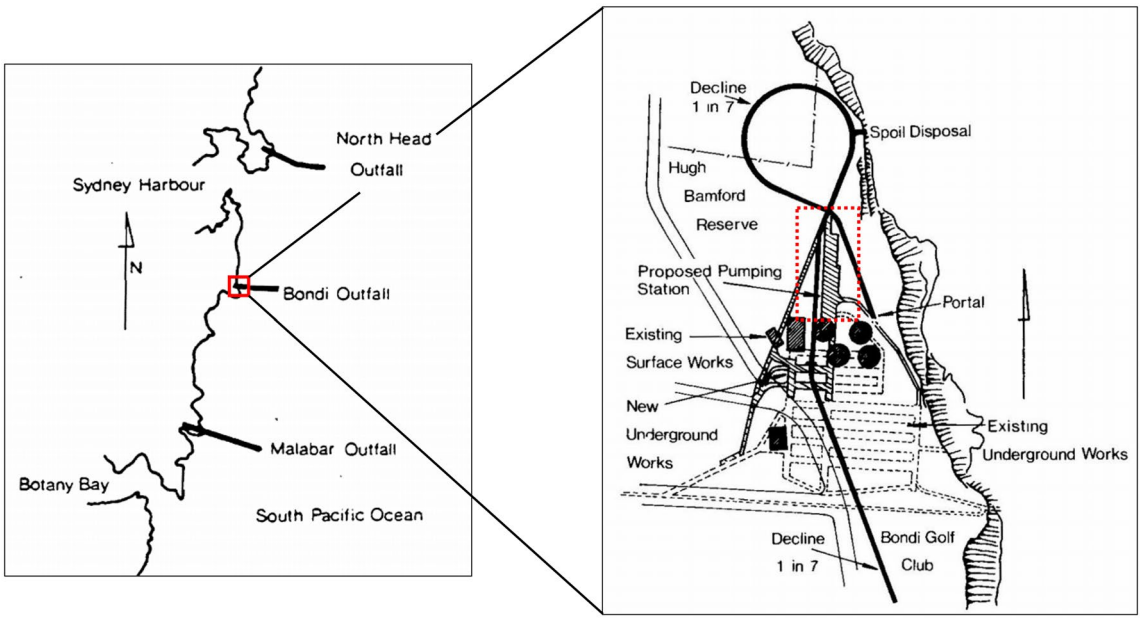

Fig. 1 Location of the North Head, Bondi, and Malabar ocean outfall tunnels (left) (modified from Nye et al. 2005). Site plan of the Bondi STP indicating proposed pumping chamber location prior to construction (right) (modified from Clancy 1984)

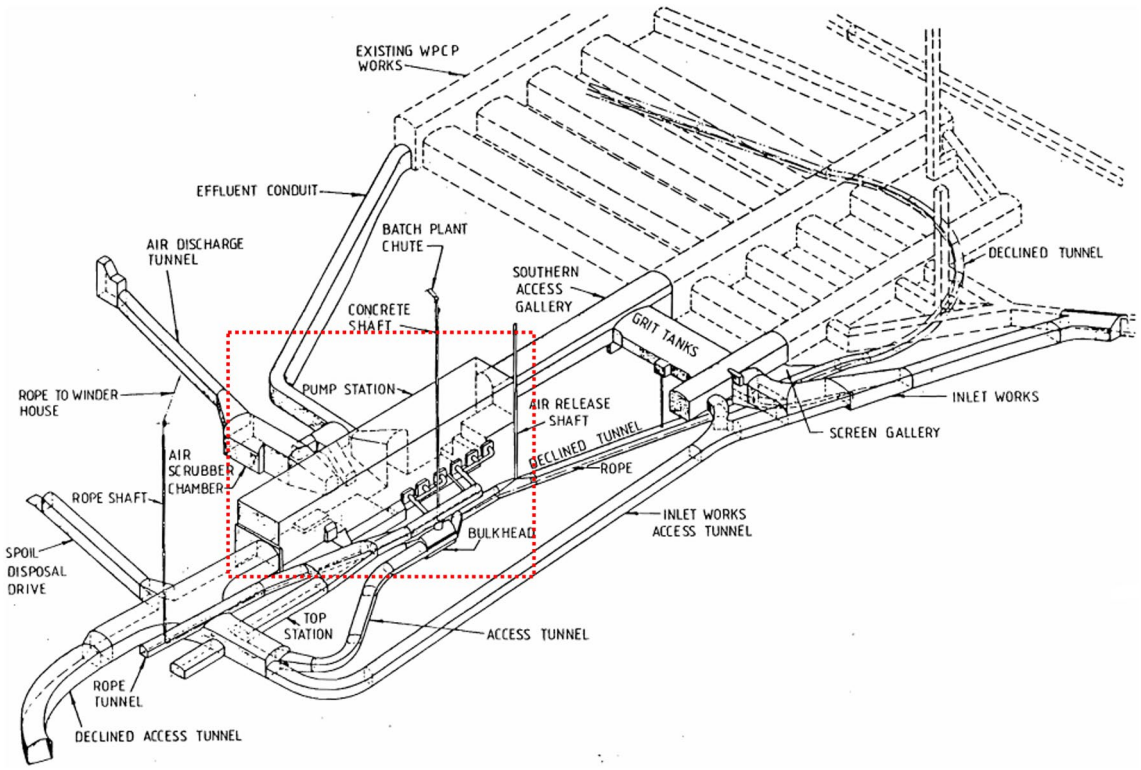

Fig. 2 Isometric view of the Bondi STP from the northwest and location of the pumping chamber (modified from Henderson and Windsor 1988)

geometries, and roof geometries to be established. First, a 4 m wide central heading was excavated by drill-and-blast through the "Unit 1 Lower Laminate", approximately 3 bolts were installed on 1.2 m spacing with faceplates, and roof extensometers and survey monuments were installed to begin displacement monitoring. Second, the right and

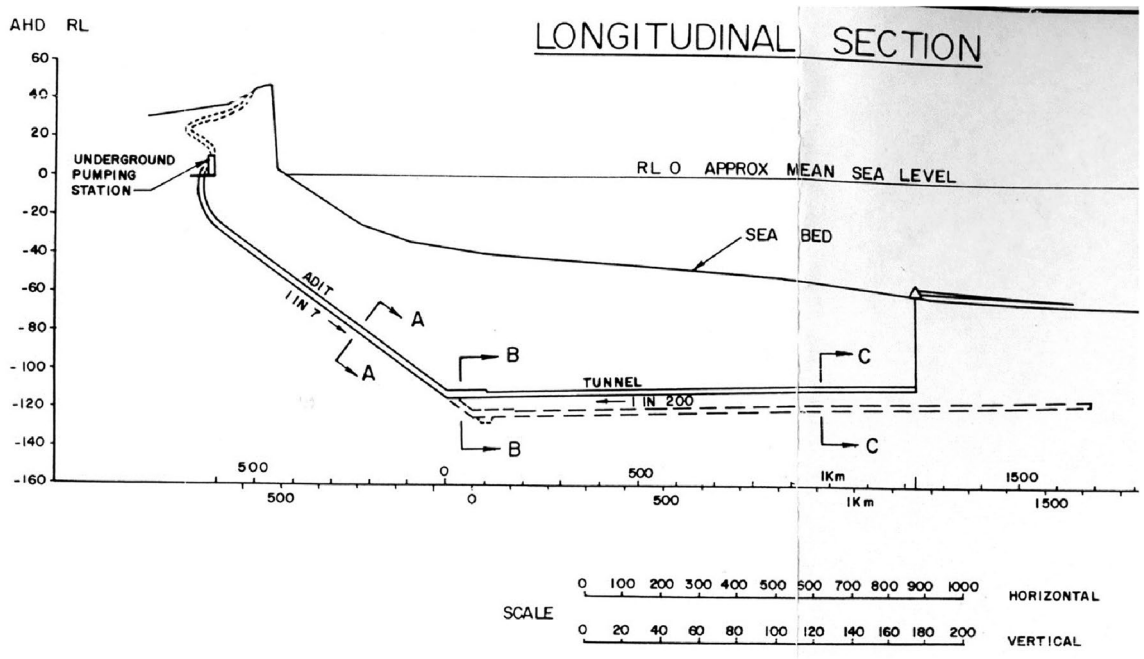

Fig. 3 Cross section of the Bondi Pumping Chamber and associated outfall runnels in the Sydney region (from P. Pells, personal communication 03/23/21)

Fig. 4 Images of typical Hawkesbury Sandstone massive facies from the North Head outfall project north of the Bondi pumping chamber (see Fig. 1) (from P. Pells, personal communication 03/23/21)

left headings were excavated, with the roof being bolted on 1.2 m spacing during excavation advance. After excavation advance, the initial 50 mm of shotcrete was applied to the entire excavation, and angled bolts were installed through the initial shotcrete in the right excavation corner to support the weaker laminate layer. Last, a final liner of 75–100 mm thick shotcrete was applied, and the remainder of the chamber was benched down via drill-and-blast to the final height of 19 m. This sequence was confirmed by engineers who helped design the excavation, however the exact timing of support installation (i.e. minutes, hours, or days) remains unverified (P. Pells, personal communication 04/03/21). Furthermore, conflicting evidence in the literature indicates that the bolts installed in the roof may have been passive (Pells and Best 1991; Pells 1993) or pretensioned to 60 kN (Henderson and Windsor 1988; Pells et al. 2018). Personal communication with P. Pells was unable to resolve this discrepancy. Previous research indicates that the difference in performance between passive and active bolts is likely to be insignificant (Boon et al. 2015), but numerical models were utilized to evaluate that hypothesis in the specific context of the Bondi Pumping Chamber excavation (see Sect. 7).

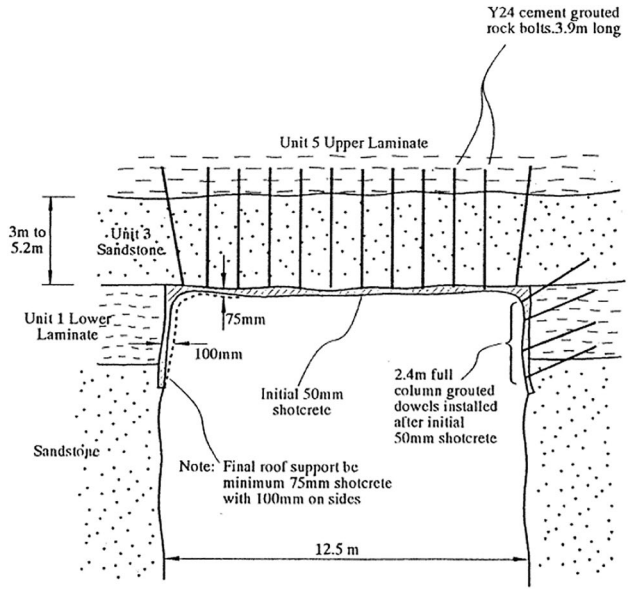

Fig. 5 Generalized dimensions, support, and local geology of the Bondi pumping chamber (from Pells 1993)

As the excavation was advanced, deflection measurements were collected by roof extensometers and surface survey points to allow for the total deflection of the roof to be recorded. Following full advancement of the central heading and installation of the roof extensometers, the surveys found that between 4 and 10 mm of total roof sag occurred at the midspan as the excavation was widened from 4 to 12.5 m and benched down to its final height of 19 m (Pells and Best 1991) (Fig. 6).

The variability in the measured roof sag is likely due to variation in the thickness of the main sandstone roof (i.e. "Unit 3 Sandstone" in Fig. 5), possible variation in support installation timing, and local geologic heterogeneity. Numerical models were used to consider and constrain the effects of support installation timing on ultimate roof deflection (see Sect. 7).

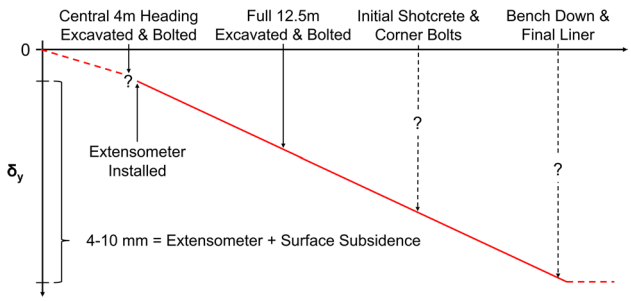

Fig. 6 Timing of measured roof displacement in relation to known excavation sequence (dashed lines and question marks indicate uncertainty in pre-instrumentation displacement and excavation sequence timing)

3.2 Rockmass Characterization

Unconfined compressive strength (UCS) testing on the sandstone from the Bondi Pumping Chamber excavation resulted in a mean UCS of 30.7 MPa and dry tangent Young's modulus of 13.8 GPa (Pells 2004). Site-specific geotechnical testing data for the Upper and Lower Laminate were not available, but data from other sites indicate that laminated shales in the Hawkesbury Sandstone formation have UCS values ranging from 1 to 40 MPa, intact rock moduli between 5 and 15 GPa, and rockmass moduli between 0.5 and 2.5 GPa, depending on the class of shale (Bertuzzi and Pells 2002). Both sandstone and laminate rock types are reported as having a unit weight of 24.0 kN/m^3 (Pells 2004). The relevant Hawkesbury formation shale (i.e. laminate) engineering properties are summarized in Table 1.

Additionally, the thickness of the "Unit 5 Upper Laminate" is uncertain, but a 1983 site investigation report indicated that the shale occurs in beds up to 6 m thick (P. Pells, personal communication 03/23/21). The shale class of the laminate units in the Bondi Pumping Chamber are not explicitly identified in the available literature, so a rockmass modulus of 1.0 GPa was assumed to reasonably approximate shale classes I–III.

Regarding discontinuity properties, Pells (1993) stated that there were two horizontal bedding planes in the sandstone roof. Furthermore, Pells and Best (1991) stated that the sandstone bedding plane spacing was 1–1.5 m. Regarding the strength and stiffness of those bedding planes, no site-specific data were available. However, Bertuzzi and Pells (2002) provided generalized Hawkesbury Sandstone rockmass parameter estimates for both bedding and joint strength and stiffness, which were used for this study (see Table 2). While a stress-dependent stiffness model for joints (e.g. Bandis 1980) may be generally applicable, the use of such a model is not necessary in this case, as the range of stresses experienced by the structures is limited.

Site-specific joint-set geometric data were obtained from a 1983 site investigation report for the Bondi Pumping Chamber (P. Pells, personal communication 03/23/21), which identified three major joint sets in addition to the bedding (Table 3). These structures and their variability are shown on a stereonet in Fig. 7a.

Table 1 Relevant intact (i.e. lab-scale) and rockmass engineering parameters for laminated shales in the regional laminated shale formations

Shale class	Intact UCS (MPa)	Intact E (GPa)	Rockmass E (GPa)
I/II	7–40	7–15	0.7–2.5
III	2–15	5–10	0.2–1.2
IV/V	1–2	––	0.05–0.5

Table 2 Relevant discontinuity strength and stiffness parameters in the regional sandstone and laminated shale deposits

Description	Thickness (mm)	Friction angle (°)	Normal stiffness (GPa/m)	Shear stiffness (GPa/m)
Bedding plane	Tight	35–45	4000	400
	1–5	30–35	200	20
	5–10	20–25	10	1
Joint	Tight	35–40	4000	400
	1	22–28	1500	150
	3	18–22	500	50

Table 3 Discontinuity orientation, persistence, spacing, and conditions noted during site investigation activities at the Bondi STP

Bondi joint set	Dip (°)	Strike (°)	Length (m)	Spacing (m)	Condition
Bedding	0–5 W	0	Continuous	0.3–5.0	Planar, clean, occasional clay seams
Set 2	90 ± 15	25 ± 10	1–5	1–3	Planar, rough, clean, fresh to slightly weathered wall rock
Set 3	90 ± 15	110 ± 10	1–5	> 3.0	Planar, rough, clean, fresh to slightly weathered wall rock
Set 4a	90 ± 10	150 ± 10	1–5	> 3.0	Planar, rough, clean, fresh to slightly weathered wall rock
Set 4b	90 ± 10	50 ± 10	1–5	> 3.0	Planar, rough, clean, fresh to slightly weathered wall rock

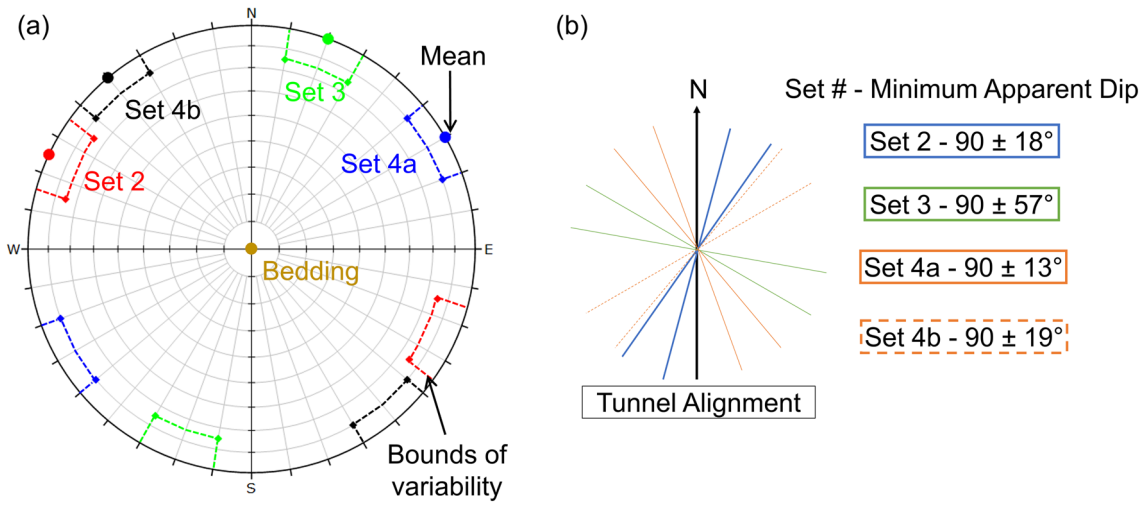

Fig. 7 Joint set upper and lower bound strike in relation to tunnel alignment and apparent dips range for each joint set in relationship to the tunnel cross section (i.e. 90°)

This complex set of three-dimensional joint orientations needed to be represented in a two-dimensional model as well as a single vertical joint spacing value to calculate rockmass modulus per Eq. (1). These joint set orientations relative to the alignment of the excavation and their apparent dip in relation to the tunnel cross-section are shown in Fig. 7b.

Finally, Hillis et al. (1999) notes that the regional in-situ stress ratio (horizontal/vertical) ranges from 1 to 2. However, the Bondi Pumping Chamber's 30 m proximity to an unconfined cliff face is assumed to result in locally minimal horizontal stress. This assumption was confirmed to be valid based on preliminary numerical model results that found horizontal stresses in the roof to be below 0.1 MPa prior to excavation advance.

4 Numerical Model Development

In order to determine an effective average joint spacing based on a discrete fracture network (DFN), to evaluate the effect of pre-tensioned versus passive bolts on roof displacement, and to assess the effect of rockmass variation on roof

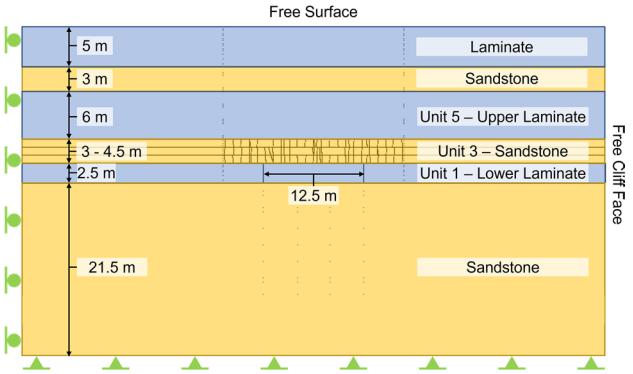

Fig. 8 Bondi pumping chamber model setup featuring boundary conditions, general lithology, roof DFN, and excavation width

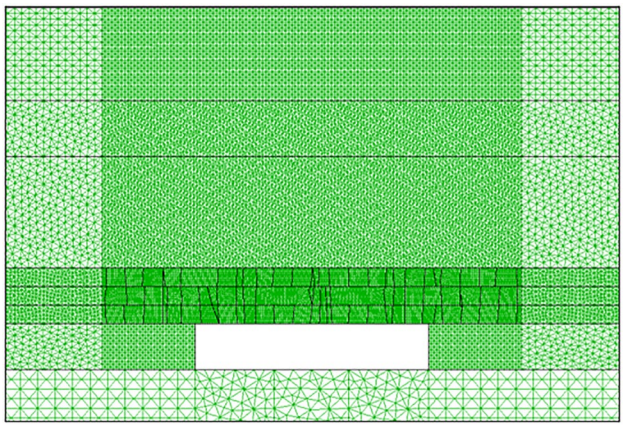

Fig. 9 Graded mesh detail example for Bondi pumping chamber numerical models prior to benching stage. Note that elastic vertical joints are used to create horizontal variation in mesh densities

displacement, multiple 2D numerical models were developed using the Universal Distinct Element Code (UDEC) version 6.0 (Itasca Consulting Group Inc. 2014). An example UDEC model geometry is depicted in Fig. 8, showing boundary conditions, as well as generalized model lithology and a stochastically generated roof DFN.

4.1 Model Boundary Conditions, Staging, & Zone Size

The modeled cliff face at the right boundary was left as a free surface and initial model stresses were set based on a $k_o = 2.0$; these stresses decayed significantly during stress initialization due to the unconfined right boundary. This simulated the release of regional elevated horizontal stress as the escarpment formed. A zero-velocity boundary condition was applied in the normal direction to the left side of the model, and a pinned (i.e. both x- and y-velocity restricted) boundary condition was used for the model bottom. The pinned boundary condition utilized at the model bottom was considered more realistic than implementing a roller boundary (i.e. only y-velocity restricted) due to the unconfined nature of the escarpment. A roller boundary effectively places a continuous joint with no shear strength, unconstrained at the escarpment end of the model, between the explicitly modeled rock at the bottom of the model and the in-situ rock that is not represented in the model (i.e. the other side of the boundary). Preliminary model runs using a roller boundary condition at the bottom of the model resulted in unrealistic tensile stresses forming on the restricted side of the model (i.e. opposite the cliff face) after stress initialization, and tensile stresses in the walls of the cavern after excavation. These tensile stresses promoted roof collapse by counteracting the formation of a competent beam.

In order to simulate the roof displacement associated with an advancing excavation, the model was run in five stages: (1) stresses were initialized and allowed to decay; (2) the 4 m central heading was excavated, and a 70% internal boundary stress was applied to the excavation interior and solved to an equilibrium solution ratio of 1.0×10^{-5} to mimic relaxation prior to bolt installation in accordance with longitudinal displacement profiles from Vlachopoulos and Diederichs (2009). This effectively corresponds to an assumption that any deformation ahead of the excavation was elastic in nature (Walton et al. 2015); (3) the central heading bolts were installed, the relaxation stress boundary was removed, and the model was run to an equilibrium solution ratio. Bolt material properties were taken from Bahrani and Hadjigeorgiou (2017) based on calibrated simulations of pull test; (4) the right and left headings were excavated simultaneously, the same stress relaxation and bolt installation procedure was repeated along the newly excavated boundary, and the model was solved to an equilibrium solution ratio; (5) the excavation was benched to its final height and solved a final time. Maximum roof midspan vertical displacement was tracked and extracted using a *history* command, and the final stress state of the immediate roof was saved for comparison to the adjusted voussoir analytical method.

The models utilized a graded mesh with smaller elements (0.125) in the immediate roof, identical to the mesh size in Abousleiman et al. (2021). Element size was doubled and quadrupled for the remainder of the model, since minimal deformation was expected away from the jointed and bolted immediate roof (Fig. 9).

4.2 Modeled Rockmass Properties

A DFN based on the set of cross-joint strikes identified in Table 3 was generated in the immediate roof beam above

Table 4 DFN geometry parameter mean values and standard deviations (sd) used in the Bondi pumping chamber model

Bondi joint set	Theta [sd] (°)	Spacing [sd] (m)	Persistence [sd] (m)	Gap [sd] (m)
Set 2	90 [6.0]	1.0 [0.0]	3.0 [0.5]	0.0 [0.0]
Set 3	90 [19.0]	6.0 [1.0]	3.0 [0.5]	0.0 [0.0]
Set 4a	90 [4.3]	4.0 [0.3]	3.0 [0.5]	0.0 [0.0]
Set 4b	90 [6.3]	4.0 [0.3]	3.0 [0.5]	0.0 [0.0]

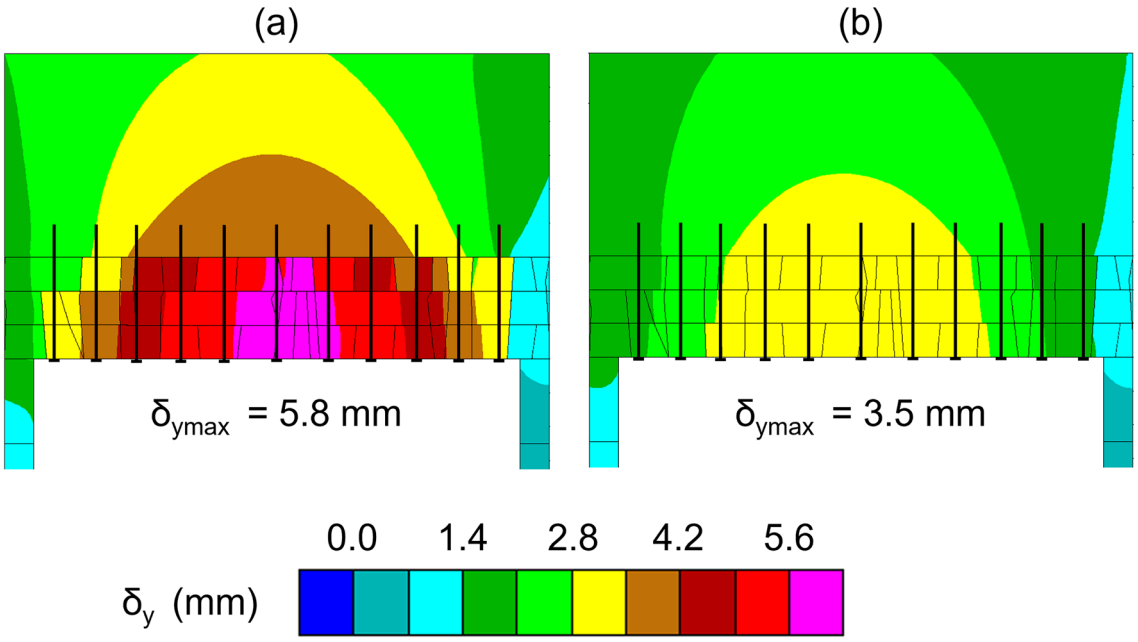

Fig. 10 Bondi pumping chamber numerical model displacement results for the lower-bound 3 m thick roof featuring **a** weaker and softer discontinuities (i.e. Case MP1) and **b** stronger and stiffer discontinuities (i.e. Case MP2)

the excavation and approximately 5 m past the horizontal bounds of the excavation (see Table 4 for DFN input parameters). Note that the minimum apparent dip shown in Fig. 8 was subtracted from the mean dip (90°) and divided by 3 to obtain the standard deviation for the DFN Theta input in Table 4.

The mean joint spacing of the superimposed DFNs listed in Table 4 and depicted in Fig. 10 was measured as 0.8 m and used in the adjusted analytical method as described in Sect. 2.

Due to the extremely shallow and low-confinement nature of the excavation, the potential for substantial intact block material yield was deemed to be insignificant, so elastic block models were utilized to study the bolted roof response. Joints were modeled using the Continuously Yielding constitutive model. Note that the DFN was restricted to the sandstone areas directly above the excavation, and the remaining sandstone was modeled as an elastic equivalent continuum with a rockmass modulus calculated using Eq. (21) from Diederichs and Kaiser (1999) based on intact sandstone elastic modulus, joint stiffness, and the mean spacing of the model generated DFNs. The mean model joint spacing was taken by calculating the average of joint spacing in each roof layer (i.e. span divided by number of cross-joints). Other model inputs associated with low uncertainty or low potential to impact the model results were not varied in the numerical modeling portion of the case study (see Table 5 for inputs common to all models).

The mixture of site-specific and more generalized formation-level engineering data required that critical inputs were tested over a range of possible values. Specifically, multiple values were tested for the reported thickness of the sandstone roof, joint distribution, and joint strength and stiffness within the sandstone roof (see Table 6 for values of model inputs that were varied).

4.3 Summary of Model Cases and Model Output Considerations

The combinations of model properties considered per Sect. 5.2 resulted in four main Bondi Pumping Chamber

Table 5 Input parameters that remained constant between Bondi pumping chamber models

Static parameters	Value
Geometry/loading	
Depth to entry (m)	17
Excavation bench height (m)	2.5
Span (m)	12.5
In-situ stress ratio	2.0
No. sandstone layers	3.0
Bolt spacing (m)	1.2
Bolt properties	See Bahrani and Hadjigeorgiou (2017)
Bolt length (m)	3.9
Mean joint spacing (m)	0.8
Block material properties	
DFN block sandstone K (GPa)	7.7
DFN block sandstone G (GPa)	5.8
Laminate K (GPa)	0.56
Laminate G (GPa)	0.42
Discontinuity material properties	
Bedding roughness (mm)	1.0
Joint roughness (mm)	1.0

numerical models: two sandstone roof thickness values, each being tested with both minimum and maximum discontinuity strengths and stiffnesses. Table 7 presents a summary of the model cases presented in this study.

Preliminary 3.0 m thick roof model behavior (Cases MP1 and MP2) deviated from expected stress behavior and prompted additional model cases (Cases M1 and M2) with bolts that did not penetrate through the roof beam. This provided a more direct comparison to the models used to develop the adjusted analytical solution (in contrast to the baseline model cases with 3.9 m bolts per Fig. 5), as the method of Abousleiman et al. (2021) did not account for the effects of partial bolt penetration into the supported roof beam (i.e. Cases M3 and M4), bolt penetration past the roof beam (Cases MP1 and MP2), shotcrete (Case MS2a), or pretensioned rockbolts (Case MS2b). The models described in Table 7 were developed to assess the potential impacts of these variations in type, timing, and geometry of support installation.

The reported displacement results (Sect. 6) from the adjusted analytical solution and numerical modeling efforts account for the timing of field displacement measurements in order to make direct comparisons. In the adjusted analytical solution, displacement is assumed to vary continuously as a function of increasing span, and this allows displacement of a 4 m span (i.e. central heading) beam to be

Table 6 Input parameters that were varied between Bondi pumping chamber models; note that discontinuity (i.e., bedding and joint) stiffness and strength variables were varied concurrently

Variable parameters	Values tested	
	Minimum	Maximum
Geometry/loading		
Sandstone roof thickness (m)	3	4.5
Discontinuity properties		
Bedding jkn/jks (GPa/m)	200/20	4000/400
Bedding initial/intrinsic friction Angle (°)	35/30	45/35
Joint jkn/jks (GPa/m)	1500/150	4000/400
Joint initial/intrinsic friction Angle (°)	28/25	45/35

Table 7 Summary of the model cases presented in this study, their relevant properties, and their stated purpose

Case	Roof thickness (m)	Bolt length (m)	Contact properties (Table 6)	Support type	Results section	Analytical comparison	Comments
MP1	3.0	3.9	Weak/soft	Passive bolts	6.2	No	Preliminary
MP2	3.0	3.9	Strong/stiff	Passive bolts	6.2	No	Preliminary
M1	3.0	2.9	Weak/soft	Passive bolts	6.2	Yes	Replaced MP1
M2	3.0	2.9	Strong/stiff	Passive bolts	6.2	Yes	Replaced MP2
M3	4.5	3.9	Weak/soft	Passive bolts	6.2	Yes	–
M4	4.5	3.9	Strong/stiff	Passive bolts	6.2	Yes	–
MS2a	3.0	2.9	Strong/stiff	Passive bolts, shotcrete, corner bolts	7.1	No	M2 with alternate support
MS2b	3.0	2.9	Strong/stiff	Pretensioned bolts	7.2	No	M2 with alternate support

subtracted from the displacement of a 12.5 m span beam for comparison to the field-measured displacements. In the numerical models, the recorded displacements are set to 0 after Stage 3 (i.e. completion of the 4 m central heading and support installation). In both cases, the reported stresses are total stresses for the 12.5 m span with no adjustment, as there were no field measurements of stress against which to make comparisons.

The timing of support installation is not identical to the models used to develop the adjusted analytical solution in Abousleiman et al. (2021), where bolts were installed prior to any beam deflection; however, the amount of pre-installation displacement is insignificant in relation to the scale of measured deflection in this case. Specifically, the modeled pre-support displacement for the 4.0 m central heading was between 0.01 and 0.02 mm. Following excavation expansion and prior to support installation in the newly excavated areas, the displacement at the midspan increased to between 0.04 and 0.05 mm.

The adjusted analytical method and numerical model results presented required no calibration and were intended to represent an approximation of what could have been produced prior to construction using available field data.

Lastly, the authors acknowledge that the use of 2D modeling software to simulate a case study with 3D structures is a major limitation of the study. This was done to facilitate comparison with the adjusted analytical method of Abousleiman et al. (2021). Nonetheless, the inability to properly account for discontinuities that are parallel/near-parallel to the 2D modeling plane could neglect localized 3D block failures and their potential impact on overall beam stability. Additionally, any potential stabilizing forces associated with irregular model-parallel fractures and out of plane stresses that might affect layer deflection are neglected.

5 Results

5.1 Layered & Bolted Voussoir Beam Analog

The adjusted voussoir beam analog was applied as summarized in Sect. 2 (see Abousleiman et al. (2021) for more details) accounting for the unmeasured displacement of the central heading (i.e. prior to installation of extensometers and expansion of the excavation from 4 to 12.5 m wide) with good agreement to the range of roof displacement observed in the field. The results are summarized in Table 8. Note that Analytical cases A1-A4 are meant to be compared to numerical model cases M1-M4.

The adjusted analytical solution results were generally consistent with the range of reported roof displacement, particularly for the lower-bound 3 m thick sandstone roof cases. Varying the triangularly distributed surcharge load from 0 to 120 kPa (i.e. the conservative value used in Pells and Best (1991)) resulted in a range of predicted displacements from 4.6 to 9.8 mm for the 3 m thick sandstone cases. Notably, the changes in contact material properties (i.e. j_{kn} reduced from 4000 to 1500 GPa/m and joint initial friction from 45° to 28°) had no noticeable effect on the voussoir analytical solution except to lower the factor of safety against sliding failure. The upper-bound roof bolted thickness (i.e. 4.5 m) underpredicted displacement as reported by Pells and Best (1991), and the $FoS_{sliding}$ decreased significantly for the minimum contact strength case (i.e. Case A3).

5.2 Numerical Model Results

Model roof displacement for the 3.0 m thick roof cases (i.e. Case MP1 and MP2) were generally consistent with both the

Table 8 Results of the adjusted voussoir analytical solution using applied to the known geometric and rockmass conditions of the Bondi pumping chamber for two different surcharge pressure cases

Case	BT (m)	Contact properties (Table 6)	δ_{max} (mm)		σ_{max} (MPa)		$FoS_{crushing}$		$FoS_{sliding}$	
			q (kPa) 0	q (kPa) 120	q (kPa) 0	q (kPa)120	q (kPa) 0	q (kPa) 120	q (kPa) 0	q (kPa)120
A1	3.0	Minimum	4.6	9.8	2.4	5.1	3.9	1.8	3.2	3.2
A2	3.0	Maximum	4.6	9.7	2.4	5.1	3.9	1.8	5.9	5.9
A3	4.5	Minimum	2.2	3.7	1.6	2.8	5.9	3.4	2.1	2.1
A4	4.5	Maximum	2.2	3.7	1.6	2.8	5.9	3.4	4.0	4.0

BT bolted thickness, *q* triangularly distributed surcharge pressure, δ_{max} maximum midspan displacement, σ_{max} maximum midspan stress, $FoS_{crushing}$ factor of safety against crushing, $FoS_{sliding}$ factor of safety against sliding

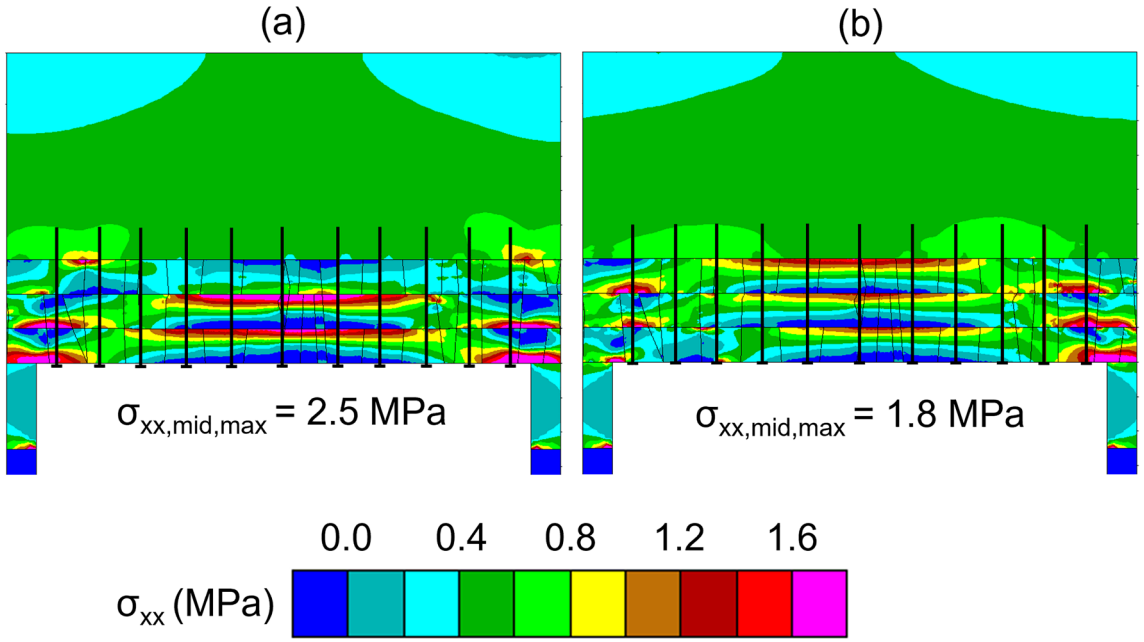

Fig. 11 Bondi pumping chamber numerical model horizontal stress results for the lower-bound 3 m thick roof featuring **a** weaker and softer discontinuities (i.e. Case MP1) and **b** stronger and stiffer discontinuities (i.e. Case MP2)

lower-bound displacement results of the adjusted voussoir beam analog and measured roof displacements (Fig. 10).

While no field stress measurements were available, model results of horizontal stress were also evaluated (Fig. 11).

Maximum midspan stress was significantly overpredicted by the adjusted voussoir analytical solution in the stronger and stiffer discontinuity case (2.4 MPa analytical versus 1.8 MPa numerical). In this case, the numerical model showed both inter-beam and intra-beam stress arching similar to that observed in the simplified models used by Abousleiman et al. (2021) (Fig. 11b). The distribution of horizontal stresses in the weaker discontinuity case was highly non-uniform with the upper layer supported in suspension (Fig. 11a). The discrepancy between the two is interpreted to be partially due to the bolt penetration into the upper laminate promoting suspension, a condition that was not tested in the development of the adjusted analytical solution. When the strong discontinuity 3.0 m thick sandstone roof model was rerun with 2.9 m long bolts (i.e. Case M2), both the displacement and stress results were more consistent with the adjusted analytical solution (Fig. 12). However, the model midspan stress was still slightly below the lower-bound estimate of the adjusted analytical solution. The idealized voussoir conditions utilized to develop the adjusted method represented the maximum stress transfer possible, with no possibility of sliding (Ran et al. 1994). Therefore, the presence of non-vertical joints (as in this case) should strictly reduce the stress arching capacity of the supported roof due to sliding (Ran et al. 1994) relative to the analytical solution prediction, as sliding results in compressive stress release.

Further evidence in support of this explanation was found in the onset of sliding failure along vertical discontinuities in roof model results with weaker and softer cross-joints (i.e. Case M1 and M3) (Fig. 13).

Calculation of $FoS_{sliding}$ assumes that the roof fails as soon as the contact strength is exceeded. However, this is clearly not the case when the joints have non-zero residual strength, as in reality. The model stresses diverge from the stress prediction based on perfectly vertical cross-joints, decreasing the applicability of the analytical $FoS_{sliding}$ in Table 8.

In 4.5 m thick roof models with stronger cross-joints (i.e. Case M4), the absence of joint sliding allowed for the model results to match the analytical solution for displacement with a surcharge load between 0 and 120 kPa, while the midspan stress results matched the adjusted analytical solution predictions for the lower surcharge load cases. This further confirms that the sub-vertical joints are decreasing the bolted roof beam's stress arching capacity relative to the maximum expected in an idealized voussoir scenario for a given amount of beam deflection (Fig. 14).

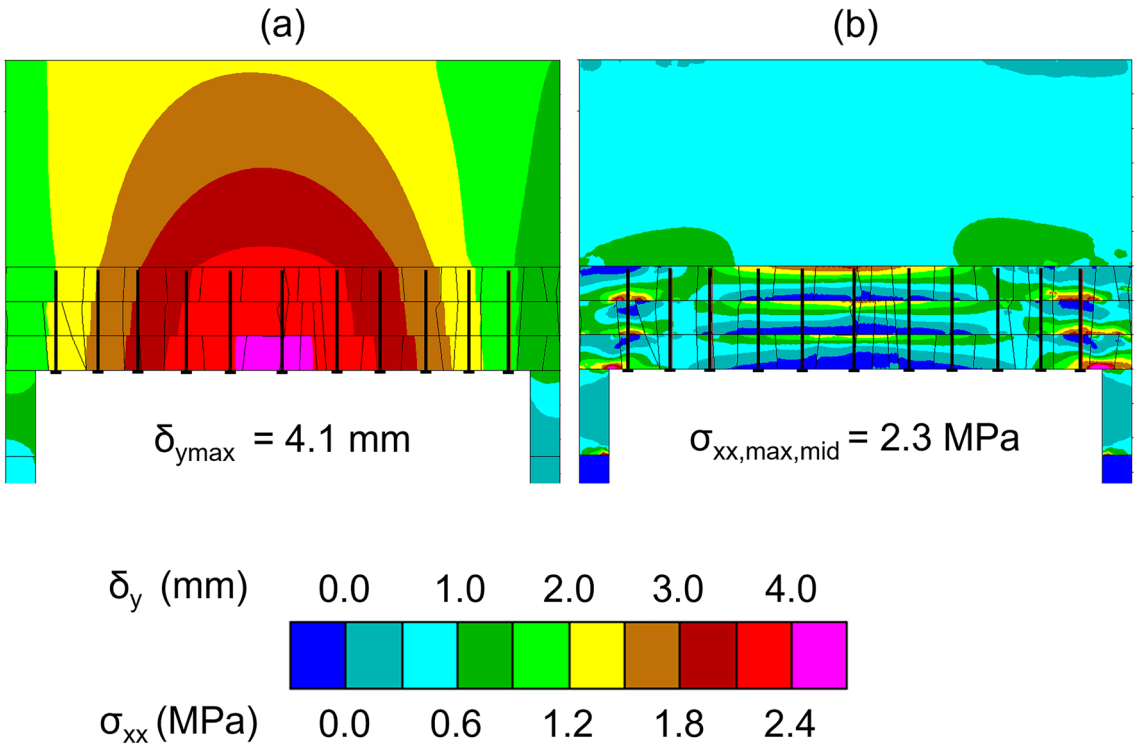

Fig. 12 Bondi pumping chamber numerical model **a** vertical displacement and **b** horizontal stress results for the lower-bound 3 m thick roof featuring stronger and stiffer discontinuities (i.e. Case M2) with shorter bolts

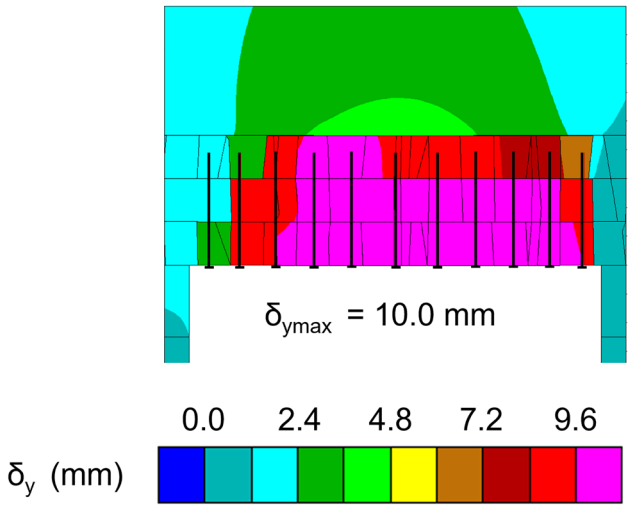

Fig. 13 Bondi pumping chamber numerical model vertical displacement results for the upper-bound 4.5 m thick roof featuring weaker and softer discontinuities (i.e. Case M3)

6 Evaluating Impacts of Support Installation Sequence Uncertainty

Due to the uncertainty regarding support installation timing and the conflicting information regarding the passive or pretensioned state of the installed roof bolts, additional numerical model cases were run to constrain the impacts of possible support configuration and timing.

6.1 Corner Support and Shotcrete

The first assessment of support installation uncertainty modeled supplemental corner support and applied 50 mm of shotcrete at the same model stage where the 12.5 m span excavation roof was supported (see Fig. 5). This represents the largest possible difference between the model sequence considered in this case study (i.e. passive roof bolt support only during beam deflection) and the earliest possible shotcrete support timing. Case M2 was analyzed due to its close match to the analytical solution and the models used to develop it. The shotcrete and supplemental corner support model was developed according to the following sequence:

1. Excavate 4 m central heading
2. 70% stress relaxation along internal excavation boundary
3. Install 3×2.9 m long, passive roof bolts on approximately 1.2 m square spacing
4. Remove internal stress boundary and solve to an equilibrium solution ratio of 1.0×10^{-5}

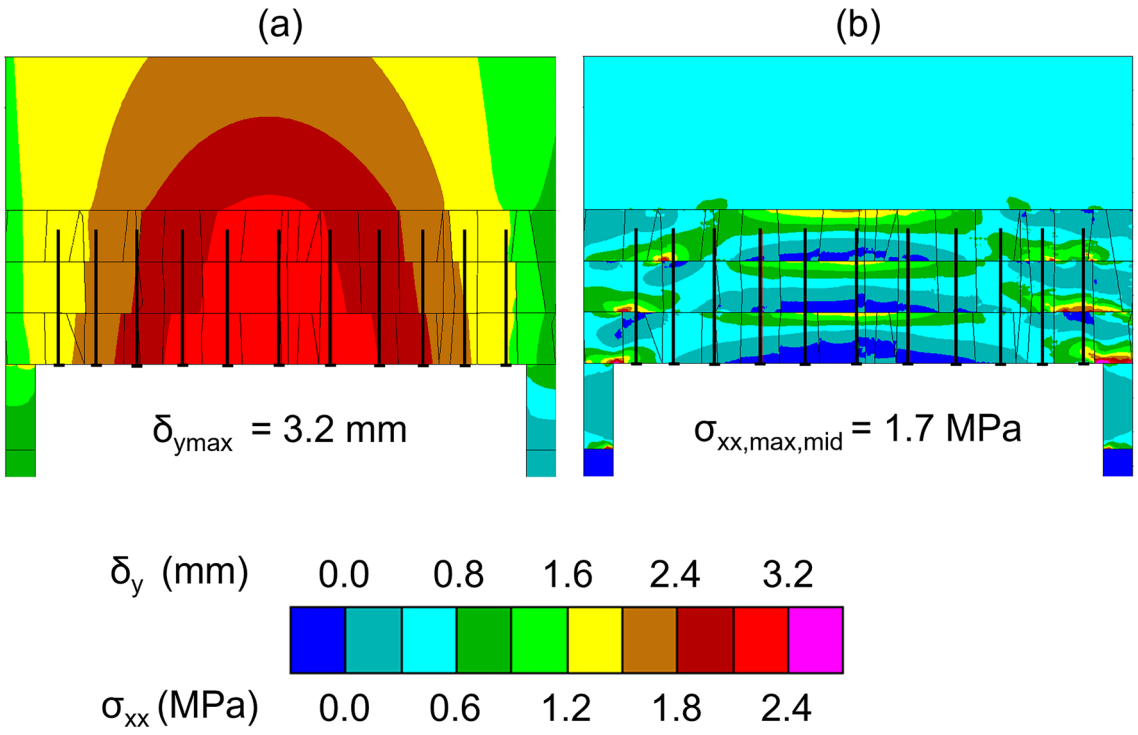

Fig. 14 Bondi pumping chamber numerical model **a** vertical displacement and **b** horizontal stress results for the lower-bound 4.5 m thick roof featuring stronger and stiffer discontinuities with shorter bolts (i.e. Case M4)

5. Set model displacement to 0 and excavate full 12.5 m span
6. 70% stress relaxation along newly excavated internal boundary
7. Install remaining 8 passive roof bolts, 4 supplemental corner bolts, and apply 50 mm of shotcrete using input parameters from Chryssanthakis et al. (1997)
8. Remove internal stress boundary and solve to an equilibrium solution ratio of 1.0×10^{-5}
9. Bench the excavation down to its final height of 19 m and solve to an equilibrium solution ratio of $1.0 \times 10)^{-5}$

This support installation timing will provide a lower-bound prediction of roof displacement, since it assumes all supplemental support is installed at the same time as the initial passive bolt support for the full excavation span. Any delay in the installation of supplemental support relative to this case can only result in higher displacements, closer to those presented in Sect. 5.2.

The addition of the supplemental support to Case M2 decreased model displacement by 0.4 mm (i.e. 9%) and model maximum midspan stress by 0.1 MPa (Fig. 15). This indicates that the presence of supplemental corner support and 50 mm of shotcrete had minimal impact on the model roof behavior. The limited impact of the added support is hypothesized to be due to the low stress conditions, flat-roof excavation geometry, and low shotcrete thickness relative to the excavation span. The minimal difference also increased confidence in the application of the analytical solution to the Bondi Pumping Chamber case study.

If the stress conditions were higher or the excavation geometry was less conducive to stress arching, the additional support (i.e. shotcrete, corner bolts) could reduce displacement further by reducing plastic deformation of intact material or sliding of individual blocks. Shotcrete liners are far more effective in a circular excavation where radial stresses put the liner into compression. In the flat-roof case, the 4 mm of displacement at the midspan is loading the thin layer of shotcrete more similar to a fixed-end beam, inducing tensile stress and reducing the support efficacy.

6.2 Pretensioned Roof Bolts

The second model variation used an identical excavation and support sequence to that presented in Sect. 3.1; however, bolts were assigned a pretension force of 60 kN in accordance with Henderson and Windsor (1988). Itasca's UDEC version 6.0 does not have built-in option to assign pretension to rockbolt structural elements as it does with cable structural elements. Cable structural elements were not appropriate as they cannot sustain any shear loading.

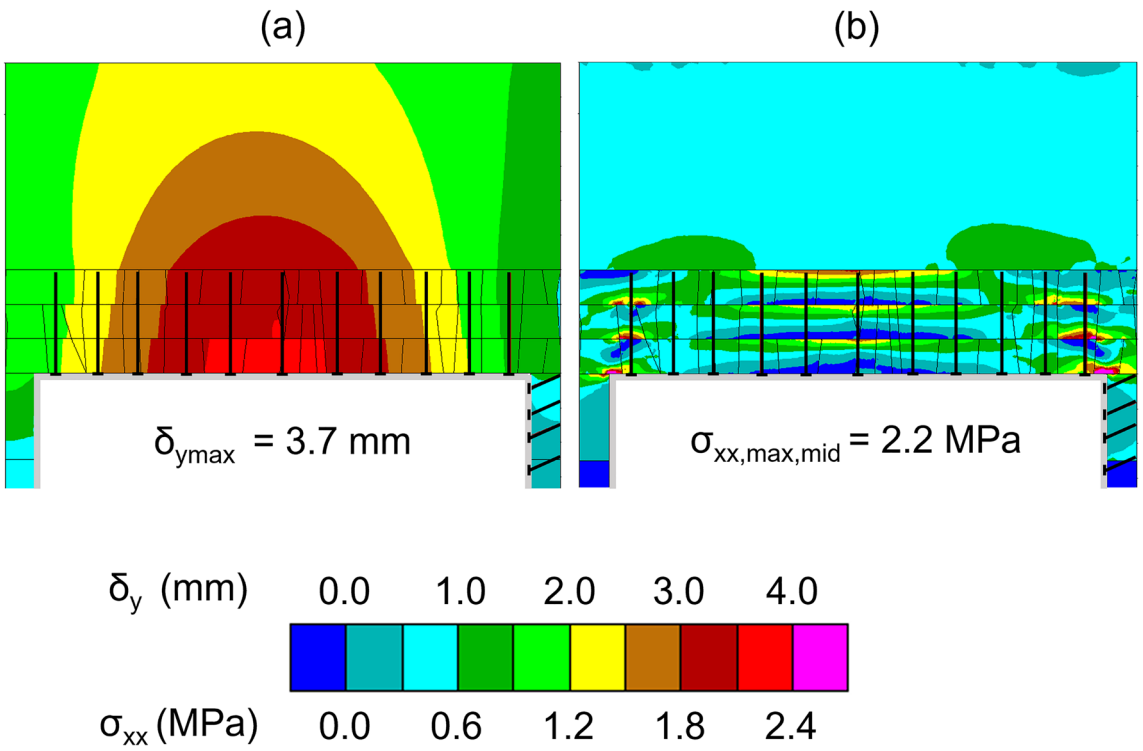

Fig. 15 Bondi pumping chamber numerical model **a** vertical displacement and **b** horizontal stress results for the lower-bound 3 m thick roof featuring stronger and stiffer discontinuities (i.e. Case M2) with supplemental corner bolts and 50 mm shotcrete liner (i.e. Case MS2a)

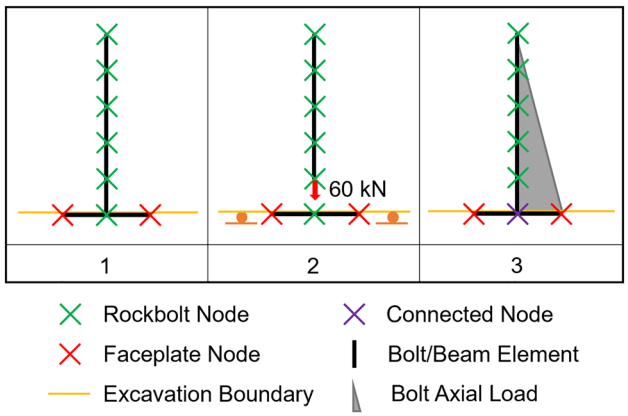

Fig. 16 Depiction of bolt pretensioning processes implemented in UDEC

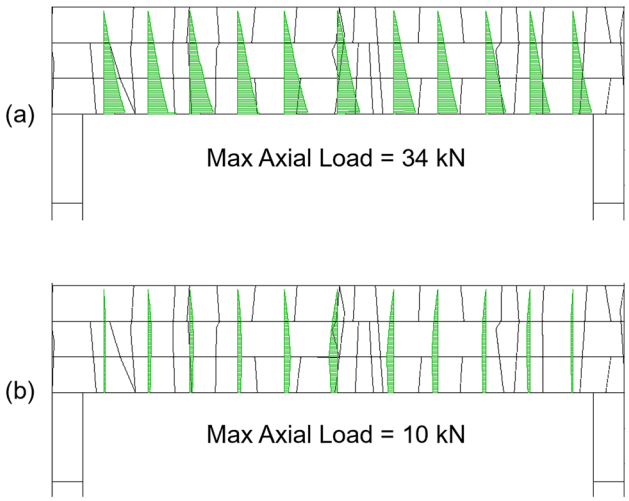

Fig. 17 Comparison of bolt axial load at final model equilibrium for **a** pretensioned bolt model (i.e. Case MS2b) and **b** passive bolts (i.e. Case M2)

Therefore, a method was developed by which pretension could be assigned to rockbolt elements using FISH code.

Bolts and faceplates were installed as described in Sect. 4.1, but the common node that the bolt and faceplate shared was not attached using the *connect* command (Fig. 16). The 70% internal stress boundary was removed, and a zero-velocity internal boundary condition was applied. Then the element (i.e. member between two nodes) between the faceplate and the second rockbolt node was deleted and a downward axial force of 60 kN was applied to the remaining rockbolt node. The model was solved to an equilibrium solution ratio of 1.0×10^{-5} and the bolt axial force was checked to ensure it was approximately 60 kN. Then the applied axial

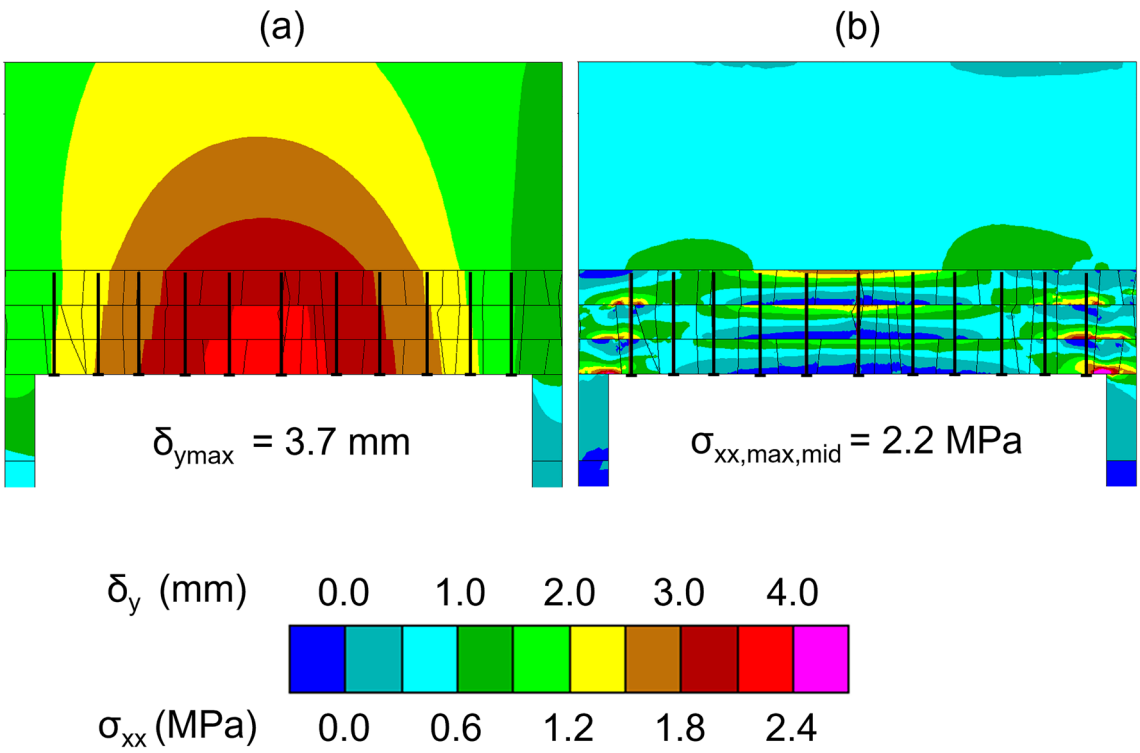

Fig. 18 Bondi pumping chamber numerical model **a** vertical displacement and **b** horizontal stress results for the lower-bound 3 m thick roof featuring stronger and stiffer discontinuities (i.e. Case MS2b) with 60 kN pretensioned bolts

force was removed from the node and the faceplate node and bolt node were reconnected with a new element; the faceplate was deleted and reinstalled using the "connect" command to attach the faceplate to the pretensioned bolt. The internal zero-velocity boundary condition was removed and the model was solved as outlined in Sect. 6.1.

This bolt tensioning function was repeated when the excavation was widened. Comparing bolt axial tension between the passive and pretensioned models at model equilibrium indicates that the pretensioning method developed was effective at maintaining bolt pretension as shown in Fig. 17, even though values decayed from 60 kN, which is a realistic behavior observed in pretensioned cable bolt elements (Itasca Consulting Group Inc. 2014).

The use of pretensioned bolts decreased model roof displacement by 0.4 mm and model maximum midspan stress by 0.1 MPa when compared to the baseline Case M2 model results (Fig. 18). This suggests that due to the competent nature of the rock and the low stress magnitudes, bolt pretensioning had a limited impact on roof behavior and the applicability of the adjusted voussoir beam analytical method.

This agrees well with the findings of Boon et al. (2015), who showed that pretensioned bolts supporting a shallow excavation in a well-jointed, competent rockmass had a minimal influence on excavation convergence.

7 Conclusions

The results of the Bondi Pumping Chamber case study highlight the practical applicability of the adjusted voussoir beam analog developed by Abousleiman et al. (2021) relative to previous voussoir beam methods when considering the effect of roof bolt support in laminated and jointed rockmasses. Rockmass parameters and construction methodology information obtained from the available literature and through personal communication with the design engineer were incorporated to develop a DFN that accounted for the apparent dip of the joint sets relative to the alignment of the tunnel. A mean joint spacing was recorded from the generated DFN and applied to the adjusted voussoir analytical method with good agreement between the analytically predicted displacement, the in-situ measurements, and the 3 m thick roof beam model cases. However, the roof displacement in the 4.5 m thick roof beam case was underpredicted by the adjusted voussoir analytical solution in relationship to the measured roof sag. This difference can be explained by multiple mechanisms including, but not limited to, non-continuous roof deformation in the field (i.e. abutment slip failure), continuous roof deformation in the direction of excavation (i.e. sag governed by

the thinnest portion of the roof), the location(s) of extensometer installation (i.e. not in the thicker portions of the roof), and the influence of joint interactions in three dimensions (i.e. due to their intersection with other joint sets sub-parallel to the excavation axis). Note that the 4.5 m thick roof beam models with strong and stiff joints agreed with the adjusted analytical solution.

The adjusted voussoir beam analog maximum midspan stress predictions were confirmed to represent an upper-bound estimate of numerically modeled beam stress due to the presence of sub-vertical joints. Overall, however, the validity of the adjusted voussoir beam analog for practical application has been demonstrated through this case study. The method provides a mechanical basis by which Young's Modulus should be reduced that can be used in lieu of overly conservative assumptions.

Importantly, this study demonstrates the voussoir beam analog has advanced beyond the critique that "perfect knowledge of a perfect rockmass" (Oliveira and Pells 2014) is required for its implementation. In particular, preliminary estimates of displacement and maximum horizontal stress in regularly bolted roofs in laminated and discontinuous rockmasses can be obtained used the adjusted analytical solution of Abousleiman et al. (2021).

Acknowledgements The views, opinions, and recommendations expressed herein are solely those of the authors and do not imply any endorsement by the ALPHA FOUNDATION, its directors and staff. Part of the modeling effort for this study was conducted as part of the first author's course of study using educational licenses of UDEC provided by Itasca Consulting, Ltd. The authors appreciate Itasca's support in this capacity. The authors also thank David Oliveira and Phillip Pells for their correspondence, guidance, and insight into the Bondi Pumping Chamber case study.

Author Contributions Rami Abousleiman: conceptualization, methodology, validation, formal analysis, investigation, data curation, writing—original draft, writing—review & editing, visualization. Sankhaneel Sinha: conceptualization, methodology, writing—review & editing. Gabriel Walton: conceptualization, methodology, resources, writing—review & editing, supervision, project administration, funding acquisition.

Funding This study was primarily sponsored by the Alpha Foundation for the Improvement of Mine Safety and Health, Inc. (ALPHA FOUNDATION). The research conducted for this study was also partially funded by the National Institute of Occupational Health and Science (NIOSH) under Grant Number 200–2016-90154.

Availability of Data and Materials Data taken from published literature (see references).

Code availability Available upon request.

Declarations

Conflict of interest There are no conflicts of interest.

References

Abousleiman R, Sinha S, Walton G (2021) Expanding application of the voussoir beam analog to horizontally bedded and passively bolted flat-roof excavations using the discrete element method. Int J Rock Mech Min Sci 148:104919

Alejano LR, Taboada J, García-Bastante F, Rodriguez P (2008) Multi-approach back-analysis of a roof bed collapse in a mining room excavated in stratified rock. Int J Rock Mech Min Sci 45:899–913. https://doi.org/10.1016/J.IJRMMS.2007.10.001

Bahrani N, Hadjigeorgiou J (2017) Explicit reinforcement models for fully-grouted rebar rock bolts. J Rock Mech Geotech Eng 9:267–280. https://doi.org/10.1016/j.jrmge.2016.07.006

Bandis S (1980) Experimental studies of scale effects on shear strength, and deformation of rock joints. PhD dissertation, University of Leeds

Beer G, Meek J (1982) Design curves for roofs and hanging-walls in bedded rock based on "voussoir" beam and plate solutions. Inst Min Metall Trans

Bertuzzi R, Pells P (2002) Geotechnical parameters of Sydney sandstone and shale. Aust Geomech J News Aust Geomech Soc 37:41–54

Boon CW, Houlsby GT, Utili S (2015) Designing tunnel support in jointed rock masses via the DEM. Rock Mech Rock Eng 48:603–632. https://doi.org/10.1007/s00603-014-0579-8

Brady BHG, Brown ET (2013) Rock mechanics: for underground mining. Springer Science & Business Media, Berlin

Carvalho JL, Carter TG (2020) Revision of the voussoir beam analogue for crown pillars. In: 54th U.S. rock mechanics/geomechanics symposium, American Rock Mechanics Association

Chryssanthakis P, Barton N, Lorig L, Christianson M (1997) Numerical simulation of fiber reinforced shotcrete in a tunnel using the discrete element method. Int J Rock Mech Min Sci Geomech Abstr 34:590. https://doi.org/10.1016/S1365-1609(97)00094-4

Clancy KG (1984) Design and Construction Planning for Sydney's Sewerage Outfalls General Report June 1984. In: Fifth Australian tunnelling conference: state of the art in underground development and construction; preprints of papers. Institution of Engineers, Australia, p 98

Diederichs MS, Kaiser PK (1999) Stability of large excavations in laminated hard rock masses: the voussoir analogue revisited. Int J Rock Mech Min Sci 36:97–117. https://doi.org/10.1016/S0148-9062(98)00180-6

Evans WH (1941) The strength of undermined strata. Am Inst Min Metall Eng 50:475–500

Fayol H (1885) Note sur les mouvements de terrain provoquée par l'exploitation des mines

He L, Zhang QB (2015) Numerical investigation of arching mechanism to underground excavation in jointed rock mass. Tunn Undergr Space Technol 50:54–67

Henderson ADD, Windsor CRR (1988) Investigations, planning and construction control I for the Sydney ocean outfalls tunnels. In: Cost effective tunnelling in the Sydney Basin: AUCTA seminar, Sydney, July 1988. Australian Underground Construction and Tunnelling Association, p 44

Hillis RR, Enever JR, Reynolds SD (1999) In situ stress field of eastern Australia. Aust J Earth Sci 46:813–825. https://doi.org/10.1046/j.1440-0952.1999.00746.x

Itasca Consulting Group Inc. (2014) UDEC-universal distinct element code, version 6.0

McQueen LB (2004) In situ rock stress and its effect in tunnels and deep excavations in Sydney. Aust Geomech 39:43–57

Nye E, Rowe A, McQueen LB (2005) Bondi STP RIAMP underground facility. In: Proceedings of the 12th Australian tunnelling

conference. Australian Underground COnstruction and Tunnelling Association, Brisbane, Qld., pp 212–221
Oliveira D, Paramaguru L (2016) Laminated rock beam design for tunnel support. Aust Geomech J 51:1–17
Oliveira D, Pells P (2014) Revisiting the applicability of voussoir beam theory for tunnel design in Sydney. Artic Aust Geomech J 49:29–44
Pells P (1993) Rock mechanics and engineering geology in the design of underground works. EH Davis Meml Lect 1993:3–21
Pells P (2004) Substance and mass properties for the design of engineering structures in the Hawkesbury sandstone. Aust Geomech 39:1–21
Pells P, Best RJ (1991) Aspects of primary support design for tunnels in the Sydney Basin. Trans Inst Eng Aust Civ Eng CE33:57–66. Int J Rock Mech Min Sci Geomech Abstr 29:261–262. https://doi.org/10.1016/0148-9062(92)90957-2
Pells P, Pells SE, Pan L (2018) On the resistance provided by grouted rock reinforcement to shear along bedding planes and joints. Aust Geomech 53:55–74
Ran JQ, Passaris EKS, Mottahed P (1994) Shear sliding failure of the jointed roof in laminated rock mass. Rock Mech Rock Eng 27:235–251. https://doi.org/10.1007/BF01020201
Shabanimashcool M, Li CC (2015) Analytical approaches for studying the stability of laminated roof strata. Int J Rock Mech Min Sci 79:99–108. https://doi.org/10.1016/j.ijrmms.2015.06.007
Sofianos AI (1996) Analysis and design of an underground hard rock voussoir beam roof. Int J Rock Mech Min Sci Geomech Abstr 33:153–166. https://doi.org/10.1016/0148-9062(95)00052-6
Sofianos AI, Kapenis AP (1998) Numerical evaluation of the response in bending of an underground hard rock voussoir beam roof. Int J Rock Mech Min Sci 35:1071–1086. https://doi.org/10.1016/S0148-9062(98)00166-1
Talesnick ML, Ya'Acov NB, Cruitoro A (2007) Modeling of a multiply jointed voussoir beam in the centrifuge. Rock Mech Rock Eng 40:383–404. https://doi.org/10.1007/s00603-006-0104-9
Tsesarsky M (2012) Deformation mechanisms and stability analysis of undermined sedimentary rocks in the shallow subsurface. Eng Geol 133–134:16–29. https://doi.org/10.1016/j.enggeo.2012.02.007
Vlachopoulos N, Diederichs MS (2009) Improved longitudinal displacement profiles for convergence confinement analysis of deep tunnels. Rock Mech Rock Eng Rock Engng 42:131–146. https://doi.org/10.1007/s00603-009-0176-4
Walton G, Diederichs MS, Punkkinen A (2015) The influence of constitutive model selection on predicted stresses and yield in deep mine pillars—a case study at the Creighton mine, Sudbury, Canada. Geomech Tunn 8:441–449. https://doi.org/10.1002/geot.201500023
Wright F (1972) Arching action in cracked roof beams. In: Fifth international strata control conference. Morgantown, West Virginia
Wright F, Mirza M (1963) Stress distribution around a vertical crack in a mine roof beam. Trans Inst Min Eng 226:174–179
Yiouta-Mitra P, Sofianos AI (2018) Multi-jointed stratified hard rock roof analysis and design. Int J Rock Mech Min Sci 106:96–108
Zhang ZX, Xu Y, Kulatilake PHSW, Huang X (2012) Physical model test and numerical analysis on the behavior of stratified rock masses during underground excavation. Int J Rock Mech Min Sci 49:134–147